International Journal of Nanoelectronics and Materials
IJNeaM
ISSN 198-5761 | E-ISSN 2232-1535

Dual Doping of Sulfur and Nitrogen Induces Hierarchical Porous Carbon from Wastes Medical Masks for Supercapacitor Electrodes

Retno Asih[a,*], Fitriani[a], Dylia Rahmadyanti[a], Haniffudin Nurdiansah[b], Norizah A. Karim[c], Dita P. Sari[d], Fathan Bahfie[e], Hideki Nakajima[f], Lukman Noerochim[b], Muhammad M. Ramli[c] and Darminto[a]

[a]*Department of Physics, Institut Teknologi Sepuluh Nopember, Surabaya 60111, Indonesia.*
[b]*Department of Material and Metallurgical Engineering, Institut Teknologi Sepuluh Nopember, Surabaya 60111, Indonesia.*
[c]*Institute of Nano Electronic Engineering, Universiti Malaysia Perlis, Lot 106,108&110, Blok A, Taman Pertiwi Indah, Jalan Kangar Alor Setar, Seriab 01000, Kangar, Perlis Malaysia.*
[d]*College of Engineering, Shibaura Institute of Technology, Saitama 337-8570, Japan.*
[e]*Research Unit for Mineral Technology, Innovation and Research National Agency Indonesia, Lampung 34111, Indonesia.*
[f]*Synchrotron Light Research Institute, 111 University Venue, Muang District, Nakhon Ratchasima 30000, Thailand.*
**Corresponding author: retno.asih@its.ac.id*

ABSTRACT

Demand for battery and supercapacitor materials rapidly increases as energy storage deployments accelerate. Waste-based supercapacitors have become a point of interest to accommodate growing demand and awareness of environmentally friendly products. This work aims to examine how doping with sulfur and nitrogen affects the morphology and structure of porous carbon synthesized from waste medical masks and the electrochemical performances of the prepared electrodes. Nitrogen- and sulfur-doped porous carbon (*a*-C:NS) is successfully obtained by solvothermal and hydrothermal processes in an autoclave followed by chemical activation using potassium hydroxide (KOH) and a carbonization procedure. Sulfur- and nitrogen-doping increase the yield compared to the directly carbonized process of the waste medical mask. The *a*-C:NS sample has a porous feature, showing the presence of S, N, O, and dominant C elements and the formation of C-S and C-N bonds. The supercapacitor electrode prepared from *a*-C:NS shows an electric double layer capacitor (EDLC)-*like* characteristic with a high specific capacitance (C_S) of ~300 F/g at the scanning rate of 5 mV/s. This study shows a possible route to transform polypropylene waste into functional materials for supercapacitor electrodes.

Keywords: *Amorphous carbon, Supercapacitor, Waste, Medical Mask, Nitrogen- and sulfur- doping.*

1. INTRODUCTION

As energy storage deployments accelerate, demand for supercapacitor devices significantly increases. Waste-derived carbon has become part of interest among materials candidates for supercapacitor electrodes as it provides an environmentally friendly route. Waste medical masks are a waste that has increased drastically along with the need to wear masks to avoid viral transmission. Medical-mask wastes cannot be recycled and are primarily treated in landfills like ordinary wastes, thus becoming an environmental problem [1,2]. Therefore, treatments are required for the remediation of this waste. One of the treatment technologies that recently attracted significant interest is transforming it into functional materials. Hence, it will enrich the value of medical mask wastes through safe reprocessing and utilization [3].

Advantageously, the medical mask is mainly made of polypropylene (PP), which is rich in carbon and has a lot of fibers and porosity, which, therefore, can be utilized to prepare porous carbon [3-5]. Porous carbon is amorphous carbon that has a high specific surface area, excellent porosity, and chemical stability, which is potentially applied in water treatment, air purification, catalysts and buffers, sensor, and energy storage technology, e.g., batteries and supercapacitors [6-8]. This compound can be produced through several methods, such as (i) activation treatment, including chemical and physical activations; (ii) catalytic activation of carbon sources using metal or organic-metal mixture; (iii) carbonization process of polymers that can be carbonized and pyrolyzed; and (iv) carbonization of aerogel polymer synthesized in supercritical dry condition [8]. Moreover, both synthetic polymers, such as phenol-formaldehyde, polyacrylonitrile resins, and plastic waste, and natural polymers, such as wood, coconut shell, biomass, and organic waste, can be utilized as carbon sources to obtain porous carbon materials [9-13]. Broad choice of raw materials makes porous carbon a functional material that is environmentally friendly and highly economically efficient [8,9].

Porous carbon materials are broadly applied in energy-storage technologies and sustainable environmental practices due to their large specific surface area, high degrees of porosity, good stability, and high conductivity [10-13]. Demands for porous carbon in energy storage technology have significantly increased along with the rapid development of electronic products. Supercapacitors based on porous carbon have been promising energy storage systems in recent years owing to their superior power density and extended cyclic capability [13,14].

The transformation of plastic waste into functional carbon materials has attracted extensive interest [3-5]. The carbonization of polypropylene has been studied in Ref. [15]. Using a chemical template in the preparation process brings a limited product, creating difficulty for application prospects. The solvothermal method combined with activation treatment has been proposed to prepare porous carbon from polypropylene [3,5]. This method introduces sulfur doping and increases the carbon yield. The resulting porous carbon presents good capacitive capability, 328.9 Fg^{-1} at 1 Ag^{-1}, with an energy density of 10.4 $Wh.kg^{-1}$, power density of 600 $W.kg^{-1}$, and capacitance retention rate of 81.1% after 3000 cycles [3]. In the case of porous carbon made from wood powders, nitrogen doping has successfully resulted in ultrahigh yield and good capacitive performance [16].

Due to the multi-step synthesis process in transforming PP wastes to porous carbon, low-yield products have become a challenge. Heteroatom doping is then proposed to overcome this problem. Introduction of heteroatom doping, like boron (B), nitrogen (N), sulfur (S), and phosphor (P), generates hierarchical porous structures [17], which is expected to be a reassuring porous architecture as it can accelerate the electrolyte ions transport [18,19]. Although porous carbon materials from PP waste have been studied [3], the influence of heteroatom doping on the porous architecture and its capacitive performance has yet to be investigated. Here, we introduce nitrogen and the sulfonation procedure to realize heteroatom doping of N and S. Nitrogen doping is expected to enhance carbon materials' electrical conductivity, wettability, and chemical stability [20]. Nitrogen and sulfur as heteroatom doping are expected to produce hierarchical porous and improve electrochemical properties, thus ultimately boosting the capacitive performance of the resulting porous carbon materials.

2. METHODOLOGY

Methods applied in this study include five stages, namely (i) solvothermal process: synthesis of sulfur-doped porous carbon (*a*-C:S), (ii) hydrothermal route: introduction of N doping into *a*-C:S, (iii) chemical activation process, (iv) carbonization process, and (v) preparation of supercapacitor electrodes from the resulting sample and testing its electrochemical performance. A flowchart of the employed method is illustrated in Fig. 1.

2.1. Synthesis *a*-C:S via a Solvothermal Process

The waste medical mask is cut into small pieces with a size of 0.5x0.5 cm, then 500 mg of the cut mask is mixed with 10 mL of sulfuric acid (H_2SO_4 98%) in an autoclave and heated at the temperature of 200 °C for 6 h. The resulting solid is then washed with chloride acid (HCl 1 M) once followed with distilled water until the pH is 7 (neutral). It is then dried at 100 °C for 12 h.

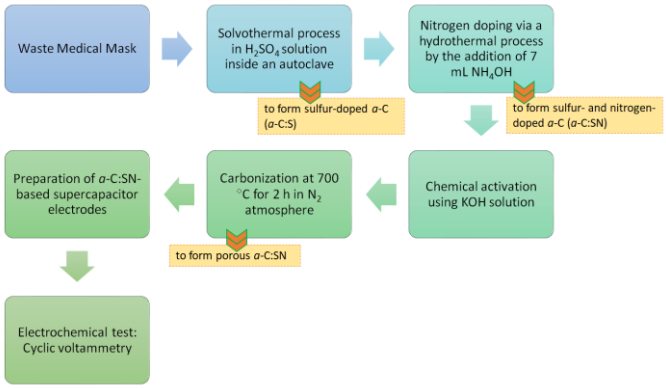

Figure 1. A schematic diagram of the methods employed in this study.

2.2. Introduction of N Doping Into *a*-C:S Via A Hydrothermal Route

N doping is added to *a*-C:S via hydrothermal processes to form N- and S-doped amorphous carbon (*a*-C:NS). 500 mg of the obtained powder is mixed with 500 mL of distilled water and stirred for 1 h, followed by ultrasonication for 1.5 h. 7 mL of ammonia (NH_4OH 25%) is added, and the hydrothermal process is carried out in an autoclave at 200 °C for 3 h. The resulting solid is then washed with HCl 1 M, followed by distilled water until it reaches neutral pH, and then dried at 100 °C for 12 h.

2.3. Chemical Activation Process

The chemical activation process is employed by mixing *a*-C:NS powders obtained in the second step with distilled water and potassium hydroxide (KOH) with a mass ratio of 1:1:3. The mixed solution is stirred and heated at 80 °C for 4 h. The resulting product is then washed with HCL 1 M, followed by distilled water until it reaches neutral pH; then, it is dried at 100 °C for 12 h.

2.4. Carbonization Process

The *a*-C:NS powders obtained in step (2.3) are carbonized at 750 °C for 2 h in the N_2 atmosphere. This process is performed in a horizontal furnace with a heating rate of 5 °C/minute and a gas flow of 0.1 L/minute. The resulting sample was washed with HCl 1 M, followed by distilled water until pH reached 7, then dried at 100 °C for 12 h. The third and fourth steps are conducted to yield *a*-C:SN with a more porous structure.

The final product is then characterized using an X-ray Diffractometer (XRD) to examine phase and amorphous features, Fourier Transform Infrared (FTIR) to evaluate chemical bonds, and Scanning Electron Microscopy with Energy Dispersive X-ray (SEM-EDX) to observe the morphology of *a*-C:NS. The mass loss behavior of samples during the heating process in the N_2 atmosphere is investigated by Thermogravimetric Analysis (TGA). Raman spectroscopy and Synchrotron Radiation X-ray Photoelectron Spectroscopy (SR-XPS) are used to study the structure of samples in more detail. The surface area and

pore size are analyzed using the Brunauer-Emmett-Teller (BET) method.

2.5. Preparation of Supercapacitor Electrodes and Electrochemical Test

The supercapacitor electrode is prepared by mixing *a*-C:NS, resulting in step (2.4), with polyvinyl alcohol (PVA) binder and acetylene black with the mass ratio of 8:1:1. The formed paste is then coated on nickel foam with a size of 1x1 cm and then dried at the temperature of 100 °C for 12 h. Furthermore, the resulting electrode is pressed and tested for its electrochemical performance using Cyclic Voltammetry (CV) with KOH 6 M as electrolytes, graphite rod as counter electrode, and saturated calomel electrode (SCE) as a reference.

The specific capacitance (Cs) of the three electrodes setup is estimated using Eq. 1 (21).

$$C = \frac{\int \mathrm{Idv}}{2\Delta \mathrm{E\ m\ v}} \quad (1)$$

C represents the specific capacitance (F/g), $\int IdV$ is an area of the CV curve, m is the total mass of active materials of the electrode (g), v describes the scan rate (mV/s), and ΔE is the potential window (Volt).

3. RESULTS AND DISCUSSION

Figure 2 presents XRD patterns of wastes medical masks and *a*-C:NS within 2θ range of 10-90°. Wastes medical mask show a characteristic pattern of PP (JCPDS card no. 66-1214), having peaks mostly between 13°-29° [22,23]. Meanwhile, the *a*-C:NS displays broad and weak intensity peaks at ~25° and ~43°, implying an amorphous feature of graphitic carbon [24,25]. This result confirms a phase transformation from PP to amorphous carbon.

The transformation of PP to amorphous carbon is also clearly observed in FTIR spectra, as shown in Fig. 3. Wastes medical mask shows a typical FTIR spectrum of PP at ~1380, ~997, and ~971 cm^{-1} [3]. Moreover, the transmittance peaks of isotactic PP also appear at wavenumbers between 1250 and 800 cm^{-1} [7]. New characteristic peaks corresponding to -OH, C=O, and C=C bonds are observed in the *a*-C:NS sample. Another peak at ~1180 cm^{-1} appears in the spectrum and is related to a sulfonic acid group that incorporates into the carbon chain of the mask [3].

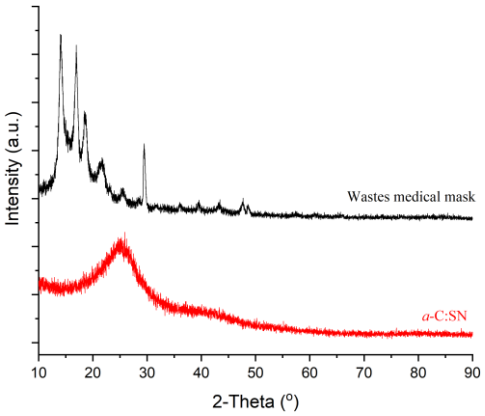

Figure 2. XRD patterns of wastes medical mask containing PP and *a*-C:NS.

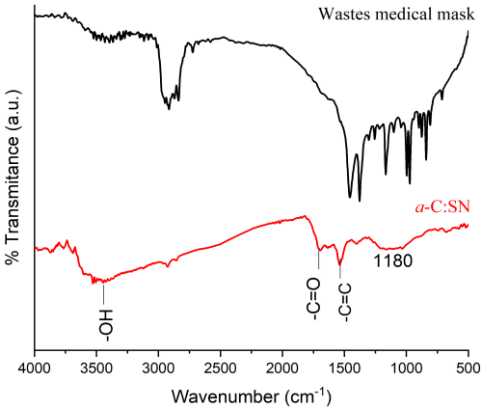

Figure 3. FTIR spectra of wastes medical mask containing PP and the *a*-C:SN sample.

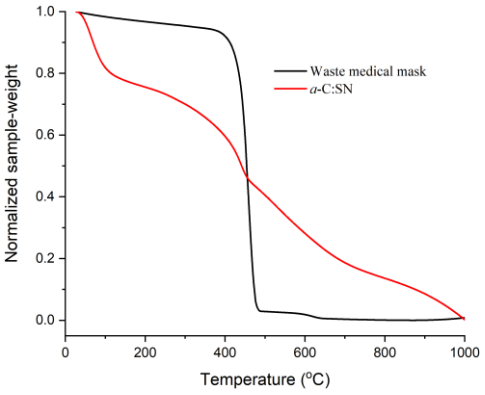

Figure 4. TGA analysis of waste medical mask and the *a*-C:NS sample heated in the atmosphere of N_2 gas.

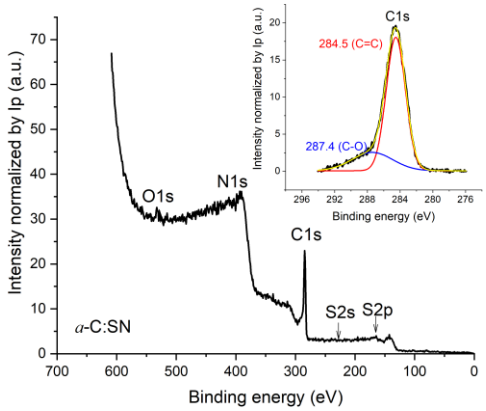

Figure 5. XPS: (a) wide and (b) C1 spectrum of the *a*-C:SN sample.

The employment of sulfur and nitrogen doping influences the yield of the sample produced. Thermal analysis using TGA shows that the mask begins to be significantly decomposed at 400 °C and is completely gone at 480 °C (Fig. 4). The *a*-C:NS sample, on the other hand, shows two steps of mass loss and a gradual degradation which indicate a progressive change to carbon-based materials. Below 200 °C, the mass loss is possibly due to a reduction in water content and a loss of sulfonate functional groups [3,5]. The decomposition of remaining raw materials then took place up to 1000 °C. Although the samples vanish at the highest applied temperature, the carbon yield is nearly 30% at ~700 °C (setup temperature of the carbonization process). It means that the S and N doping via solvothermal and hydrothermal methods enhance the sample yield compared to when the mask was just burned in the N_2 atmosphere.

To analyze bonds and hybridization states of the obtained *a*-C:NS, synchrotron X-ray photoemission spectroscopy (XPS) measurement was employed at beamline 3.2, SLRI, Thailand. The XPS wide spectrum of *a*-C:NS (Fig. 5) confirms the present of C1s, O1s, S2s, S2p, and N1s peaks. The S1s peak could not be observed due to a limit in the photon energy of the apparatus. Deconvolution of the C1s XPS spectrum results in two peaks at 284.5 and 287.4 eV, which are assigned to the C=C bond with sp^2 hybridization and C-O bond, respectively [26]. One can see that the C=C bond is dominant having a relative percentage of ~77%.

Figure 6 shows SEM images of the *a*-C:NS. Porous tube-like particles are observed. By closely looking at the particle (Fig. 6b), significant amounts of nano- to micro-sized porous appear at the surface of the particles, and they seem to be connected. This structure implies the existence of hierarchical pores within a particle [7]. SEM with EDX also confirms the presence of C, O, N, and S elements in the sample with the relative %wt of 53.2%, 39.9%, 3,9%, and 2.9%, respectively. These elements are distributed evenly, as shown in the elemental mapping of Fig. 5c. The %wt of O and S is comparable with the previous report by Hu and Lin, 2021 [3], which shows remarkable potential for supercapacitor applications even though without the addition of N doping.

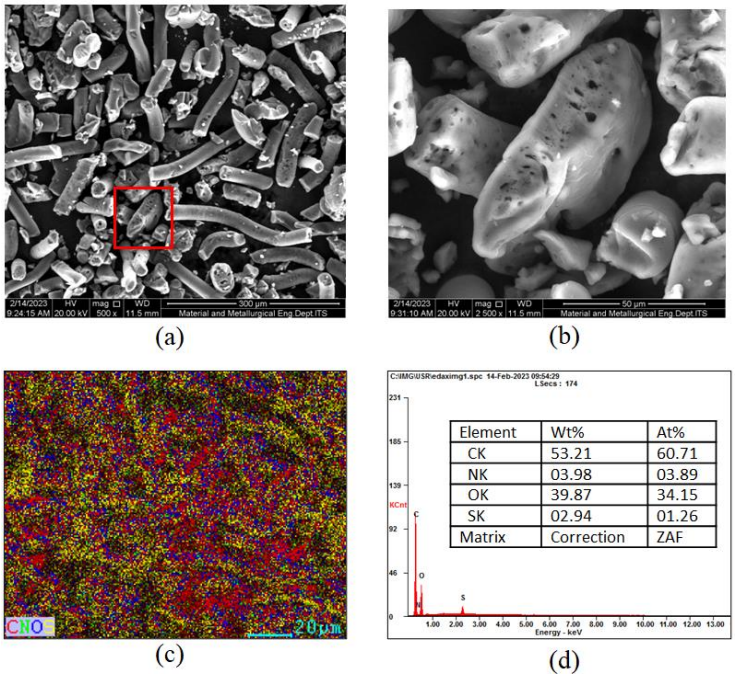

Figure 6. SEM images of the *a*-C:SN sample: (a) with the magnification of 500x, (b) a close view of porous particles, (c) elemental mapping of (a) showing the presence of C, N, O, and S elements, and (d) relative wt% and at% of each element estimated using EDX.

BET was performed to estimate pores size and specific surface area with a degassing time of 1 h. The full isotherm curve of *a*-C:NS looks like the type-IV of IUPAC BET adsorption even though the close loop is not achieved (not shown here). It was found that the *a*-C:NS sample has a specific surface area of 50.2 m^2/g, pore volume of 0.05 cc/g, and pore size of approximately 2.2 nm. The pore size is commensurable to the reported S-doped porous carbon [3], but its specific surface area is smaller. N doping could possibly affect pore formations. Further study by varying N doping is necessary to

understand the role of N doping in the specific surface area of samples.

The Raman spectrum of *a*-C:NS is illustrated in Fig. 7, showing the present of D- and G- peaks, a characteristic of carbon-based compounds. The D-peak is related to a disordered structure or defects, while the G-peak corresponds to graphitic structure with sp^2 hybridization [27]. The D- and G-peak are observed at the Raman shift of 1333.4 and 1591.9 cm^{-1}, respectively. The ratio of D- and G-peak, I_D/I_G, is approximately 1, indicating that the defects' concentration is relatively equal to that of graphitic structures. The absence of a 2D peak indeed confirms an amorphous characteristic and the observed SEM images.

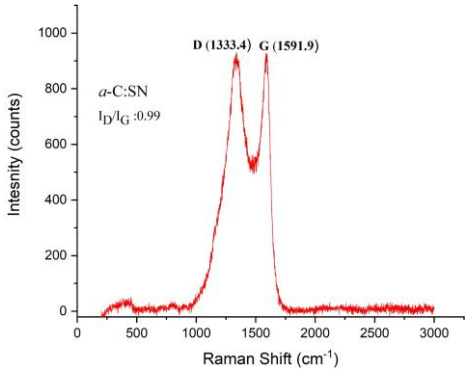

Figure 7. The Raman spectrum of *a*-C:NS shows the presence of D- and G-peaks.

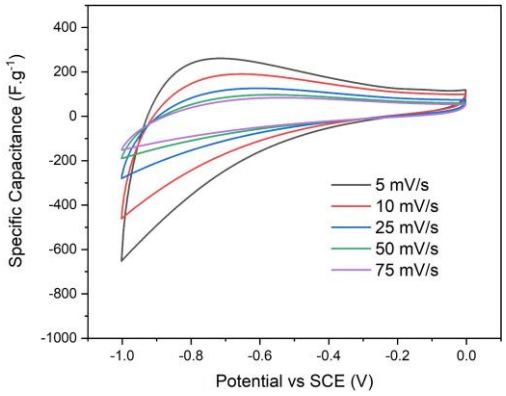

Figure 8. Cyclic voltammetry (CV) curve of the *a*-C:NS electrode at different scan rates.

After successfully synthesizing *a*-C:NS, we then prepared the electrode and examined the cyclic voltammetry (CV) curve. Figure 8 presents the CV curve of the *a*-C:NS-based electrode. All curves show an asymmetric rectangular-like shape or acute triangle shape between -1.0 V and 0 V, indicating an EDLC-*like* feature. Some reasons probably cause the asymmetric shape, namely the sample has a low active surface area and uneven material distribution, as well as the use of nickel foam as a current collector in the KOH solution resulting in a reaction to form $Ni(OH)_2$, which causes changes in the shape of the curve due to redox reactions [28]. Among these reasons, a low active surface area is confirmed from the results of the BET analysis.

The area of CV curves is enhanced by decreasing the scan rate, indicating an increase in the specific capacitance by reducing the scan rate. Applying Eq. 1, the estimated C_S at 5 mV/s is ~315 Fg^{-1}. The value is consistent with that reported in S-doped porous carbon [3].

4. SUMMARY

Dual doping (S and N) of hierarchical porous carbon (*a*-C:NS) is successfully synthesized from waste medical masks. The transformation phase from PP to amorphous carbon is confirmed using XRD and FTIR. Functional groups of C=C, C=O, and C-O are present in the obtained *a*-C:NS. S and N doping increases the amount of carbon yield produced. Supporting the FTIR data, XPS analysis confirms the existence of a dominant C=C bond with sp^2 hybridization and C-O/C-S bond in the samples. The *a*-C:NS particles have a tube-like structure with significant porous at their surface. The nano-sized porous with the approximate size of 2 nm are connected, forming a hierarchical structure. Moreover, SEM-EDX signifies the C, O, N, and S elements exist and are distributed evenly in the samples. The Raman spectrum shows a typical carbon-based compound having D- and G-peak, in which the number of defects is relatively equal to that of graphitic structures. The CV curve of the *a*-C:NS electrode shows an asymmetric rectangular-like shape, indicating an EDLC-*like* characteristic with a specific capacitance of ~315 Fg^{-1} at 5 mV/s. This study shows that introducing heteroatom doping of N and S generates a high yield in transforming waste masks to *a*-C:NS that can potentially be applied as supercapacitor electrodes. Further study of current charging-discharging behaviors is necessary to confirm the retention rate of the electrode.

ACKNOWLEDGMENTS

This work is supported by ATU-Net Young Research Grant 2022/2023 awarded to RA, NAK, DPS, and D. We acknowledge all staff at the beamline 3.2a SLRI Thailand for the assistance of XPS measurements.

REFERENCES

[1] Fonseca, W. S., Meng, X. H., Deng, D. (2015). Trash to treasure: transforming waste polystyrene cups into negative electrode materials for sodium ion batteries. ACS Sustain Chem Eng. Volume: 3. 2153–2159.

[2] Pol, V. G. (2010). Upcycling: converting waste plastics into paramagnetic, conducting, solid, pure carbon microspheres. Environ Sci Technol. Volume: 44. 4753–4759.

[3] Hu, X. and Lin, Z. (2021). Transforming waste polypropylene face masks into S-doped porous carbon as the cathode electrode for supercapacitors. Ionics. Volume 27. 2169–2179.

[4] Chellamani, K., Veerasubramanian, D., Balaji, R. V. (2013). Surgical face masks: manufacturing methods and classification. J. Acad. Indust. Res. Volume: 2. 320–324.

[5] Yuwen, C., Liu, B., Rong, Q., Zhang, L., Guo, S. (2022). Porous carbon materials derived from discarded COVID-19 masks via microwave solvothermal method for lithium-sulfur batteries. Science of the Total Environment. Volume: 817. 152995.

[6] Guan, L., Pan, L., Peng, T., Gao, C., Zhao, W., Yang, Z., Hu, H., Wu, M. (2019). Synthesis of biomass-derived nitrogen-doped porous carbon nanosheets for high performance supercapacitors, ACS Sustain. Chem. Eng. Volume: 7. 8405−8412.

[7] Wang, C., Xiong, Y., Wang, H., Sun, Q. (2018). All-round utilization of biomass derived all-solid-state asymmetric carbon-based supercapacitor, J. Colloid Interface Sci. Volume: 528. 349−359.

[8] Li, B. (2020). Progress on Synthesis and Applications of Porous Carbon Materials. International Journal of Electrochemical Science. Volume: 15. 1363-1377.

[9] Chen, Z., Wei, W., Ni, B.-J., Chen, H. (2022). Plastic waste derived carbon materials for green energy and sustainable environmental applications. Environmental Functional Materials. Volume: 1 Issue: 1. 34-48.

[10] Zhai, Z., Zhang, L., Du, T., Ren, B., Xu, Y., Wang, S., Miao, J., Liu, Z. (2022). A review of carbon materials for supercapacitors. Materials & Design. Volume: 221. 111017.

[11] Wang, H., Liu, Z., Hui, L., et al. (2020). Biomass-derived Porous Carbon Materials for Supercapacitor Electrodes: A Review. Paper and Biomaterials. Volume: 5 Issue: 2. 60-75.

[12] Wang, Y., Zhang, L., Hou, H. et al. (2021). Recent progress in carbon-based materials for supercapacitor electrodes: a review. J Mater Sci. Volume: 56. 173–200.

[13] Luo, X.-Y., Chen, Y., Mo, Y. (2021). A review of charge storage in porous carbon-based supercapacitors. Volume: 36. 49-68.

[14] Shi, C., Hu, L., Hou, J., Guo, K., Zhai, T., Li, H. (2018). Alkali metal boosted atom rearrangement in amorphous carbon towards crystalline graphitic belt skeleton for high performance supercapacitors. Energy Storage Mater. Volume: 15. 82−90.

[15] Song, C. Y., Hao, L., Zhang, B. Y., Dong, Z. Y., Tang, Q. Q., Min, J. K., Zhao, Q., Niu, R., Gong, J., Tang, T. (2020). High-performance solar vapor generation of Ni/carbon nanomaterials by controlled carbonization of waste polypropylene. Sci. China Mater. Volume: 63. 779–793.

[16] Wang, C., Wang, H., Dang, B., Wang, Z., Shen, X., Li, C., Sun, Q. (2020). Ultrahigh yield of nitrogen doped porous carbon from biomass waste for supercapacitor. Renewable energy. Volume: 156. 370-376.

[17] Wu, T., Jing, M., Tian, Y., Yang, L., Hu, J., Cao, X., Zou, G., Hou, H., Ji, X. (2019). Surface driven energy storage behavior of dual heteroatoms functionalized carbon material. Adv. Funct. Mater. Volume: 29. 1900941.

[18] Guan, L., Pan, L., Peng, T., Qian, T., Huang, Y., Li, X., Gao, C., Li, Z., Hu, H., Wu, M. (2019). Green and scalable synthesis of porous carbon nanosheet-assembled hierarchical architectures for robust capacitive energy harvesting. Carbon. Volume: 152. 537−544.

[19] Pan, L., Wang, Y., Hu, H., Li, X., Liu, J., Guan, L., Tian, W., Wang, X., Li, Y., Wu, M. (2018). 3D self-assembly synthesis of hierarchical porous carbon from petroleum asphalt for supercapacitors. Carbon. Volume: 134. 345−353.

[20] H. Zhang, Y. Ling, Y. Peng, J. Zhang, S. Guan, Nitrogen-doped porous carbon materials derived from ionic liquids as electrode for supercapacitor, Inorganic Chemistry Communications 115 (2020) 107856.

[21] Liu, M., Niu, J., Zhang, Z., Dou, M., Wang, F. (2018). Potassium compound-assistant synthesis of muti-heteroatom doped ultrathin porous carbon nanosheets for high performance supercapacitors. Nano Energy. Volume: 51. 366-372.

[22] Ariyoshi, S., Hashimoto, S., Ohnishi, S., Negishi, S., Mikami, H., Hayashi, K., Tanaka, S., Hiroshiba, N. (2021). Broadband terahertz spectroscopy of cellulose nanofiber-reinforced polypropylenes. Materials Science & Engineering B. Volume: 265. 115000.

[23] Lotz, B. (2014). A new ε crystal modification found in stereodefective isotactic polypropylene samples. Macromolecules. Volume: 47(21). 7612-7624.

[24] Wu, H., Dong, Z., Sun, J., Ding, K. (2023). Boosting the adsorption capacity of activated carbon prepared from *Amygladus communis* shells using physicochemical coactivation method. Biomass Conversion and Biorefinery. https://doi.org/10.1007/s13399-023-04093-0.

[25] Priyanto, B., Asih, R., Ardiani, I.S., Laila, A.Z., Nadiyyah, K., Romadhon, B., et. al. (2021). Hydrogenated amorphous carbon films from palmyra sugar. Journal of Renewable Materials. Volume: 9(6). 1087-1098.

[26] Ristiani, D., Asih, R., Astuti, F., Baqiya, M.A., Kaewhan, C., Tunmee, S., Nakajima, H., Soontaranon, S., Darminto. (2022). Mesostructural study on graphenic-based carbon prepared from coconut shells by heat treatment and liquid exfoliation. Heliyon. Volume: 8. e09032.

[27] Hong, J., Park, M. K., Lee, E. J., Lee, D., Hwang, D. S., Ryu, S. (2013). Origin of new broad Raman D and G peaks in annealed graphene. Scientific Report. Volume: 3. 2700.

[28] Salleh, N. A., Kheawhom, S., Mohamad, A. A. (2020). Characterizations of nickel mesh and nickel foam current collectors for supercapacitor application. Arabian Journal of Chemistry. Volume: 13 Issue:8. 6838-6846.